2005-10-04

Ablation of MEKK4 kinase activity causes neurulation and skeletal patterning defects in the mouse embryo

Amy N. Abell
University of North Carolina at Chapel Hill

Et al.

MOLECULAR AND CELLULAR BIOLOGY, Oct. 2005, p. 8948–8959 Vol. 25, No. 20
0270-7306/05/$08.00+0 doi:10.1128/MCB.25.20.8948–8959.2005

Ablation of MEKK4 Kinase Activity Causes Neurulation and Skeletal Patterning Defects in the Mouse Embryo

Amy N. Abell,[1,6] Jaime A. Rivera-Perez,[2,6] Bruce D. Cuevas,[1,6] Mark T. Uhlik,[1,6] Susan Sather,[3] Nancy L. Johnson,[1,6] Suzanne K. Minton,[1,6] Jean M. Lauder,[4,6] Ann M. Winter-Vann,[1,6] Kazuhiro Nakamura,[1,6] Terry Magnuson,[2,6] Richard R. Vaillancourt,[5] Lynn E. Heasley,[3] and Gary L. Johnson[1,6]*

Departments of Pharmacology,[1] Genetics,[2] and Cell and Developmental Biology[4] and Lineberger Comprehensive Cancer Center,[6] University of North Carolina School of Medicine, Chapel Hill, North Carolina 27599-7365; Department of Pharmacology, University of Colorado Health Sciences Center, 4200 East Ninth Ave., Denver, Colorado 80262[3]; and Department of Pharmacology and Toxicology, University of Arizona College of Pharmacy, Tucson, Arizona 85721[5]

Received 27 April 2005/Returned for modification 23 May 2005/Accepted 15 July 2005

Skeletal disorders and neural tube closure defects represent clinically significant human malformations. The signaling networks regulating normal skeletal patterning and neurulation are largely unknown. Targeted mutation of the active site lysine of MEK kinase 4 (MEKK4) produces a kinase-inactive MEKK4 protein (MEKK4^{K1361R}). Embryos homozygous for this mutation die at birth as a result of skeletal malformations and neural tube defects. Hindbrains of exencephalic MEKK4^{K1361R} embryos show a striking increase in neuroepithelial cell apoptosis and a dramatic loss of phosphorylation of MKK3 and -6, mitogen-activated protein kinase kinases (MKKs) regulated by MEKK4 in the p38 pathway. Phosphorylation of MAPK-activated protein kinase 2, a p38 substrate, is also inhibited, demonstrating a loss of p38 activity in MEKK4^{K1361R} embryos. In contrast, the MEK1/2–extracellular signal-regulated kinase 1 (ERK1)/ERK2 and MKK4–Jun N-terminal protein kinase pathways were unaffected. The p38 pathway has been shown to regulate the phosphorylation and expression of the small heat shock protein HSP27. Compared to the wild type, MEKK4^{K1361R} fibroblasts showed significantly reduced phosphorylation of p38 and HSP27, with a corresponding heat shock-induced instability of the actin cytoskeleton. Together, these data demonstrate MEKK4 regulation of p38 and that substrates downstream of p38 control cellular homeostasis. The findings are the first demonstration that MEKK4-regulated p38 activity is critical for neurulation.

Mitogen-activated protein kinases (MAPKs) can be divided into five distinct groups that include extracellular signal-regulated kinase 1 (ERK1) and ERK2, c-Jun N-terminal kinase (JNK), p38, ERK3 and ERK4, and ERK5 (10, 34). Each MAPK is activated by MAPK kinases (MAP2Ks). ERK1 and ERK2 are phosphorylated by MEK1 and MEK2 and are primarily activated by growth-promoting stimuli. JNK is activated by its MAP2Ks, MAPK kinase 4 (MKK4) and MKK7, whereas p38 is primarily activated by MKK3 and MKK6 (MKK3/6) but can be phosphorylated by MKK4 under some circumstances (4). JNK and p38 are mainly activated by stress stimuli and cytokines but can also be stimulated by growth factors. MAP2Ks are in turn regulated by MAPK kinase kinases (MAP3Ks). MEK kinase 4 (MEKK4) is a MAP3K that regulates p38 and JNK through the phosphorylation of the MAP2Ks MKK3 and MKK6 and MKK4 and MKK7, respectively (11, 31). The physiological role of MEKK4 is poorly defined, and the pathways that promote MEKK4 signaling to MAPKs are largely unknown.

Vertebrate development is orchestrated by cell-cell interactions and cytokine gradients that regulate intracellular signaling networks. We have discovered that MEKK4 expression is regulated during development and is a critical node for the control of neural tube closure and skeletal patterning in the developing mouse embryo. In this report, we investigated the function of MEKK4 in development by the targeted inhibition of MEKK4 kinase activity. The MEKK4 gene was altered by the targeted mutation of the active site lysine to an arginine, thereby eliminating phosphotransferase activity such that the expressed MEKK4^{K1361R} protein is unable to activate MAP2Ks. Expression of kinase-inactive MEKK4 inhibited MKK3/6 and p38 signaling and enhanced apoptosis in the hindbrains of mutant mice. Recently, deletion of the MEKK4 gene has been shown to result in exencephaly and spina bifida (6). This phenotype was attributed to a modest decrease in phosphorylation of MKK4 in the hindbrains of knockout embryos (6). Similar to the MEKK4 knockout, MEKK4 kinase-inactive embryos exhibit exencephaly and spina bifida. However, loss of phosphorylation of MKK4 was not observed in MEKK4 kinase-inactive embryos or in fibroblasts derived from these embryos. Instead, we observed inhibition of MKK3 and MAPK-activated protein kinase 2 (MAPKAPK-2) in both mutant hindbrains and fibroblasts. Additional defects not observed in the MEKK4 knockout including rib and vertebral malformations and significant infertility were found with the kinase-inactive MEKK4 mice, consistent with the prediction that kinase-inactive MEKK4 would be able to influence signaling as an inhibitory mutant in a stronger and more dramatic

* Corresponding author. Mailing address: Department of Pharmacology, University of North Carolina, 1106 Mary Ellen Jones Bldg., CB 7365, Chapel Hill, NC 27599-7365. Phone: (919) 843-3107. Fax: (919) 966-5640. E-mail: gary_johnson@med.unc.edu.

way than a traditional knockout where the protein was not expressed. The findings uniquely define MEKK4 as a critical node required for normal development of the mouse embryo, and its kinase activity is important for regulation of the MKK3/p38/MAPKAPK-2 pathway.

MATERIALS AND METHODS

In situ hybridization. An N-terminal MEKK4 riboprobe was generated by BamHI digestion of hemagglutinin (HA)-MEKK4 in pCMV5 (11). The 2-kb BamHI fragment corresponding to nucleotides 105 to 2096 of murine MEKK4 was subcloned into pcDNA3(−) in both the forward and reverse orientations, resulting in both antisense and sense orientations under the T7 promoter. The riboprobe to brachyury was generated as previously described (36). In situ hybridization was performed as previously described (33). Digoxigenin-labeled probes at 1 μg/ml were hybridized to either whole-mount embryos or 8- to 10-μm-thick cryosections on glass slides as previously described (24). Whole embryos or sections were incubated with alkaline-phosphatase antidigoxigenin antibodies, followed by incubation with BM purple (Boehringer Mannheim) or nitroblue tetrazolium–5-bromo-4-chloro-3-indolylphosphate solution (Roche).

Generation of MEKK4^{K1361R} mice. Genomic DNA encoding exons 18 through 23 was PCR cloned from 129Sv wild-type (wt) mouse DNA. A 3.5-kb fragment encoding exons 18 to 21 was inserted at the 5′ end of the targeting vector Osdupdel (a gift from O. Smithies). Two mutations were generated in exon 21. A silent mutation introduced an SacI site in codon 1357, from CTG to CTC. In codon 1361, a single-nucleotide change from AAG to AGG produced the replacement of the active site lysine by an arginine. A 2.5-kb fragment encoding exons 22 to 23 was inserted at the 3′ end of the targeting vector. The neomycin resistance gene was in the reverse orientation. Outside the region of homology, the thymidine kinase gene was present for negative selection. The targeting construct was electroporated into 129Sv embryonic stem (ES) cells. Homologous recombination in two ES cell clones was confirmed by Southern blot analysis with a probe outside the region of homology and by PCR from outside the region of the targeting vector. Southern blot analysis was performed using standard techniques with a 500-bp probe to intron 23 using primers 5′ CGTTCTGAGCAGT TGCACTGGAAG 3′ and 5′ CCTACAATCAACATGCACACCCATC 3′. ES cells were injected into C57BL/6 blastocysts. Founder males were mated with 129Sv females (Taconic), and heterozygotes were crossed. Germ line transmission was verified by Southern blot analysis as described above and by PCR. PCR primers in exons 21 and 22, respectively, were 5′ GACACAGGGGAGCTGAT GGCCATGAGGGAG 3′ and 5′ GTGAAGCTCCACGCCAAAATACCG 3′. Experiments were performed on embryos and mice generated from MEKK4^{K1361R} heterozygote crosses in a mixed C57BL/6 × 129/SvE background. The *neo* cassette was not excised from the MEKK4^{K1361R} germ line. Several studies have shown the ability of the *neo* cassette to disrupt gene splicing, thus abrogating expression of the protein. Western blotting of lysates from multiple primary cell types showed equal protein expression in MEKK4^{K1361R} cells relative to that in the wild type, demonstrating that the *neo* cassette does not interfere with MEKK4^{K1361R} expression. Further, total RNA was isolated from primary cells, and reverse transcription-PCR demonstrated no significant difference in message size in MEKK4^{K1361R} cells relative to that of the wild type. All experiments using animals were performed in compliance with all federal and institutional policies.

Skeletal preparations. For staining of cartilage and bone, embryonic day 18.5 (E18.5) fetuses were prepared as previously described (7). Cartilage was detected with Alcian blue 8GX (Sigma) and bone was detected with Alizarin red S (Sigma).

Hindlimb micromass cultures. E11.5 embryos from MEKK4$^{K1361R/wt}$ crosses were isolated, and limbs were dissected and cultures prepared as previously described (3). Cultures were stained with Alcian blue to detect cartilage.

Preparation of E14.5 primary MEFs. Primary mouse embryo fibroblasts (MEFs) were prepared from embryos isolated at E14.5. Head, limbs, liver, and heart were removed. Embryos were dissociated by passage three times through an 18-gauge needle, followed by trypsinization at 37°C. Cells were cultured in Iscove's modified Dulbecco's medium containing 10% heat-inactivated fetal bovine serum, 1% penicillin, and 1% streptomycin. Experiments were performed with both primary and spontaneously immortalized cells. Fibroblasts from multiple wild-type and MEKK4^{K1361R} littermate embryos were examined with nearly identical results. A total of 200 μg of MEF lysate was probed with an affinity-purified rabbit polyclonal antibody to full-length murine MEKK4.

Embryology and histology. Depending on the age of the embryo, tail or yolk sac samples were used to genotype embryos. For histology, fetuses were isolated at E18.5, fixed whole, paraffin embedded, sectioned, and stained with hematoxylin and eosin by standard methods. For terminal deoxynucleotidyltransferase-mediated dUTP-biotin nick end labeling (TUNEL) and phospho-antibody staining, embryos were isolated on E9.5 and fixed in 4% paraformaldehyde for 4 h. Embryos were processed as previously described for in situ hybridizations. TUNEL staining was performed on cryosections according to the manufacturer's specifications (Roche). For phospho-MKK3/6, phospho-MKK4, phospho-MEK1/2, and phospho-MAPKAPK-2 staining, cryosections were permeabilized for 10 min in 0.1% Triton in Tris-buffered saline, pH 7.4. Sections were washed, blocked in 10% donkey serum, and incubated overnight with anti-phospho-specific antibodies diluted 1:500 in Tris-buffered saline and 5% bovine serum albumin. Sections were washed and incubated with DAPI (4′,6′-diamidino-2-phenylindole; 0.04 ng/ml) and Cy3 donkey anti-rabbit diluted 1:500. Imaging was performed using an Axiovert 200 M microscope from Zeiss (Germany) and imaging software from Intelligent Imaging Innovations (Denver, Colo.). To measure fluorescence intensity, autofluorescence was subtracted from all images. Then, the mean fluorescence intensity of each antibody staining was measured in the entire hindbrain along a two-cell thickness of the neuroepithelium lining the ventricles. Statistical significance was determined by Student's *t*-test analysis.

Western blot analysis, immunoprecipitations, and kinase assays. MEFs were treated as described in the figure legends. For total-cell lysates, cells were lysed in buffer A containing 20 mM Tris (pH 7.4), 150 mM NaCl, 1 mM EDTA, 1 mM EGTA, 1% Triton-X, 1 mM phenylmethylsulfonyl fluoride, 1 mM sodium vanadate, 0.05 mM dithiothreitol, 1 μg/ml leupeptin, and 17 μg/ml aprotinin. A total of 15 μg of lysate was subjected to Western blotting with phospho-specific antibodies against p38, JNK, ERK, MKK3/6, MKK4, MAPKAPK-2, and heat shock protein HSP-27 (Cell Signaling) or with antibodies recognizing total p38 (11), JNK (Cell Signaling), MKK3, MKK4, and HSP27 (Santa Cruz), and actin (Sigma). Tumor necrosis factor alpha (TNF-α) was used at a concentration of 5 ng/ml (R&D Systems). Densitometry was measured with NIH Image.

293 cells were cultured in Dulbecco's modified essential medium supplemented with 10% fetal bovine serum, 1% penicillin, and 1% streptomycin. Transfections were performed in 60-mm dishes using Lipofectamine Plus reagent (Invitrogen) according to the manufacturer's specifications for 24 to 36 h. cDNAs were as previously described (11). Cells were harvested as described above for MEFs in buffer A. A total of 500 μg of lysate was immunoprecipitated for 1 h with anti-HA (12CA5) antibody, followed by incubation with protein G-Sepharose (Zymed) for 1 h. Immunoprecipitates were washed three times with cold lysis buffer and once with cold kinase buffer containing 20 mM HEPES (pH 7.4), 10 mM $MgCl_2$, 1 mM dithiothreitol, 0.1 mM sodium vanadate, 10 mM β-glycerophosphate, and 0.5 mM ATP. Reaction mixtures were incubated at 30°C for 20 min. Lysates and immunoprecipitates were probed with anti-FLAG (Sigma), anti-HA (12CA5), anti-phospho-MKK3/6 antibody, and anti-phospho-MKK4 antibody.

Thermal challenge of primary fibroblasts. Primary wild-type and MEKK4^{K1361R} fibroblasts between passages three and five were utilized. For analysis of MAPK and HSP27 phosphorylation, cells were incubated at 42°C for the indicated times. Cells were lysed and probed as described above. For analysis of cell morphology, cells were plated on glass coverslips for 24 h. Cells were either untreated or preconditioned by incubation at 42°C for 30 min and allowed to recover for 24 h. Then, cells were either untreated or exposed to lethal heat shock at 45°C for 45 min. Cells were fixed for 10 min in 3% paraformaldehyde, permeabilized in phosphate-buffered saline containing 0.1% Triton X for 6 min, and stained with rhodamine phalloidin and DAPI. Imaging was performed using an Axiovert 200 M microscope as described above. Imaging software from Intelligent Imaging Innovations was used to perform nearest-neighbor deconvolution on 0.1-μm sections.

RESULTS

MEKK4 expression during development. Expression of MEKK4 during development was demonstrated by in situ hybridization analysis that revealed a changing pattern of MEKK4 gene expression at E8.5, 10.5, and 15.5. With the exception of the allantois that lacked MEKK4 staining, MEKK4 was expressed throughout the embryo at E8.5. MEKK4 expression was especially strong in the developing neural folds at E8.5 (Fig. 1A). At E10.5, MEKK4 was prominently expressed along the ventral spinal cord (Fig. 1B) and in

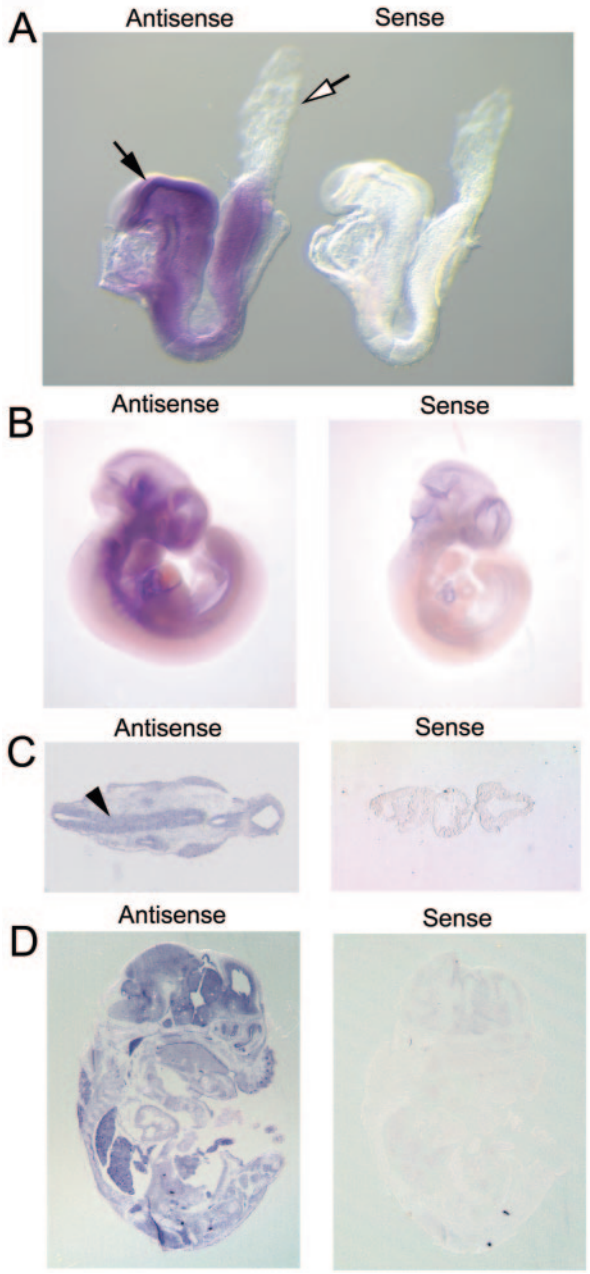

FIG. 1. MEKK4 expression during embryonic development visualized by in situ hybridization with a RNA probe to the N-terminal half of MEKK4. (A) Whole-mount embryo in situ hybridization for MEKK4 at E8.5. The solid arrow indicates neural folds, and the open arrow indicates the allantois. (B) Whole-embryo in situ hybridization for MEKK4 at E10.5. (C) In situ hybridization for MEKK4 in cryosections isolated at E10.5. The arrowhead denotes neuroepithelium. (D) In situ hybridization for MEKK4 in cryosections of embryos isolated at E15.5.

the neuroepithelium (Fig. 1C). By E15.5, MEKK4 was expressed in most tissues and organs of the embryo (Fig. 1D).

Generation of kinase-inactive MEKK4 mice. To test for the requirement of MEKK4 kinase activity, we created a mouse strain that expresses a kinase-inactive MEKK4 instead of the wild-type protein. The MEKK4 gene was mutated by replacement of the active-site lysine at position 1361 with an arginine ($MEKK4^{K1361R}$), producing an inactive kinase (Fig. 2A). Inactivation of the kinase activity of MEKK4 was validated both in vitro and in vivo. In an in vitro kinase assay, the wild-type MEKK4 kinase domain phosphorylated both His-MKK6 (Fig. 2B) and glutathione *S*-transferase (GST)-MKK4 (Fig. 2C). In contrast, $MEKK4^{K1361R}$ failed to phosphorylate either His-MKK6 (Fig. 2B) or GST-MKK4 (Fig. 2C). Furthermore, Flag-$MEKK4^{K1361R}$ was unable to stimulate either of its downstream effectors, JNK or p38, in vivo. Wild-type Flag-MEKK4 expression increased JNK (not shown) and p38 (Fig. 2D) phosphorylation. In contrast, although Flag-$MEKK4^{K1361R}$ was expressed at levels similar to that of wild-type Flag-MEKK4, Flag-$MEKK4^{K1361R}$ did not stimulate phosphorylation of either JNK (not shown) or p38 (Fig. 2D). With homologous recombination, two ES cell clones harboring the $MEKK4^{K1361R}$ gene were generated (Fig. 2E) and used to produce two independent mouse lines whose genotypes were confirmed by Southern analysis (not shown) and PCR (Fig. 2F). Importantly, Western blotting of lysates from MEFs isolated from homozygous E14.5 $MEKK4^{K1361R}$ or wild-type embryos demonstrated the expression of $MEKK4^{K1361R}$ and $MEKK4^{wt}$ proteins at comparable levels (Fig. 2G), so that differences in phenotypes found between $MEKK4^{K1361R}$ and wild-type mice would be attributable to the loss of MEKK4 kinase activity and not MEKK4 expression. During propagation of the $MEKK4^{K1361R}$ mouse colony, a non-Mendelian ratio of homozygous $MEKK4^{K1361R}$ mice was observed. At 3 weeks of age, only 9% of the pups were homozygous for the $MEKK4^{K1361R}$ gene (Table 1), suggesting that the kinase activity of MEKK4 plays an important role in development. Embryos isolated in timed breedings at early and late gestation times revealed the expected numbers of $MEKK4^{K1361R}$ embryos even at E18.5, suggesting the pups were dying perinatally (Table 1). Male mice homozygous for $MEKK4^{K1361R}$ that survived to adulthood were found to be infertile due to reduced sperm count and motility (not shown). Thus, we used animals generated from heterozygous crosses, allowing littermate controls for all the studies.

$MEKK4^{K1361R}$ embryos exhibit skeletal and neural tube defects (NTDs). Skeletal defects including asymmetric sternocostal associations, scoliosis, and vertebral malformations were the most common phenotypes associated with homozygous expression of $MEKK4^{K1361R}$. Seventy-five percent of the fetuses homozygous for $MEKK4^{K1361R}$ exhibited misalignment of sternocostal associations (Fig. 3A, B, and D). Only 5 to 8% of heterozygote fetuses showed this phenotype (Fig. 3D), but when present the misalignment of sternocostal associations in heterozygotes was often exaggerated with severe curvature of the sternum and missing ribs (Fig. 3C). In addition to defective rib attachment, vertebral malformations were observed, as shown by the prominent curvature of the spine of a heterozygote fetus (Fig. 3F and H), compared to a normal wild-type control (Fig. 3E and G). Skeletal defects were not due to defective chondrogenesis, as Alcian blue staining of micromass cultures derived from E11.5 limb buds showed that chondrogenesis was identical in $MEKK4^{wt}$, $MEKK4^{K1361R/wt}$, and $MEKK4^{K1361R}$ fetuses (not shown). Additionally, scoliosis of the axial skeleton (Fig. 3J) and bone remodeling of the tail (Fig. 3K) were detected in x-rays of adults homozygous for $MEKK4^{K1361R}$, compared to wild-type controls (Fig. 3I).

As described above, homozygous expression of $MEKK4^{K1361R}$

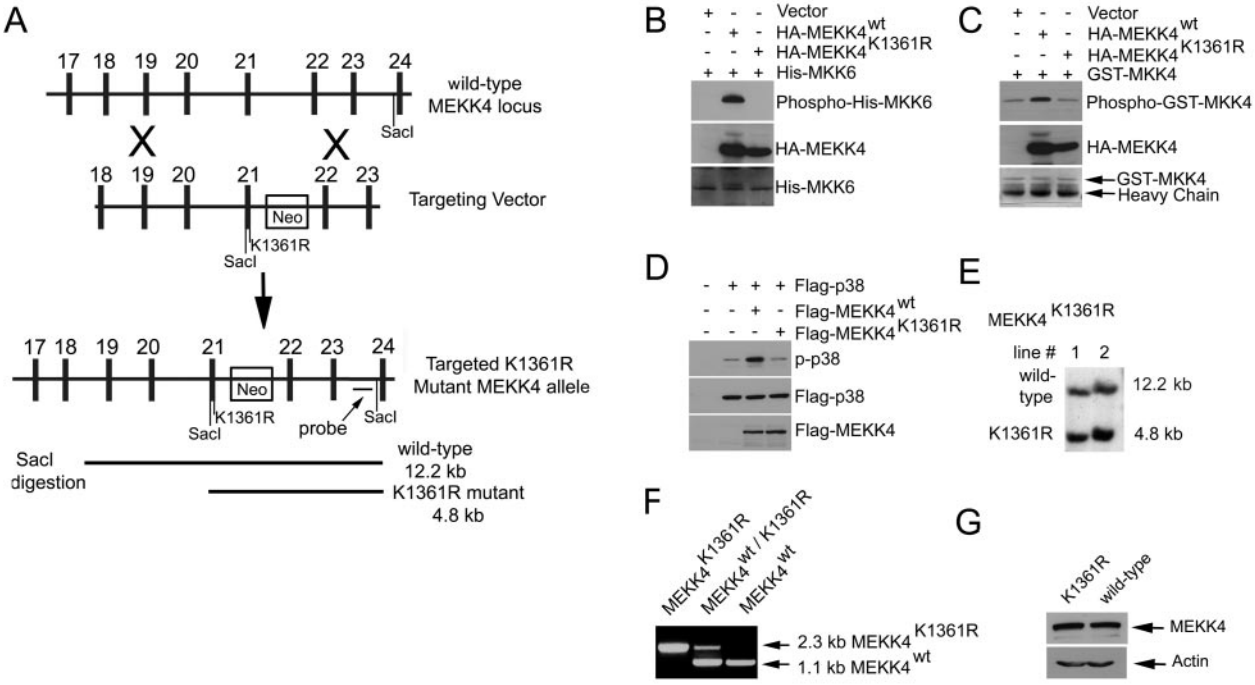

FIG. 2. Targeted replacement of the MEKK4 gene with a full-length kinase-inactive MEKK4^{K1361R}. (A) Schematic diagram of MEKK4 gene, the targeting vector, and the targeted allele. Two mutations were generated in exon 21. One silent mutation engineered a new SacI restriction site in exon 21, and the second mutation produced the replacement of the active-site lysine at position 1361 by arginine, resulting in a full-length inactive kinase. The neomycin resistance positive selection marker was inserted in the reverse orientation in intron 21. The location of the hybridization probe is indicated. Digestion of genomic DNA with SacI produces the indicated fragments. (B) Mutation of the active site lysine of MEKK4 (MEKK4^{K1361R}) disrupts the ability of MEKK4 to phosphorylate its substrate MKK6. 293 cells transfected with the HA-MEKK4^{wt} kinase domain or HA-MEKK4^{K1361R} kinase domain were immunoprecipitated with anti-HA antibody and incubated with purified kinase-inactive His-MKK6. Phosphorylation of His-MKK6 was detected with anti-phospho-MKK3/6 antibody. The total HA-MEKK4 kinase domain was detected with an anti-HA antibody. To show equal loading of substrate, Coomassie staining of the His-MKK6 substrate is shown. (C) Mutation of the active-site lysine of MEKK4 (MEKK4^{K1361R}) disrupts the ability of MEKK4 to phosphorylate its substrate MKK4. 293 cells were transfected and immunoprecipitated as described in the legend to panel C and then incubated with inactive GST-MKK4. Phosphorylation of GST-MKK4 was detected with anti-phospho-MKK4 antibody. The total HA-MEKK4 kinase domain was detected with an anti-HA antibody. To show equal loading, the GST-MKK4 substrate was stained with Ponceau. (D) MEKK4^{K1361R} is unable to activate p38. 293 cells were cotransfected with Flag-p38 and either Flag-MEKK4^{wt} or Flag-MEKK4^{K1361R}, and blots were probed as indicated. (E) Southern blot analysis of SacI-digested genomic DNA from two independent ES cell lines that were injected into C57BL/6 blastocysts and used to generate two independent heterozygous MEKK4^{K1361R} mouse lines. (F) PCR analysis of genomic DNA isolated from tail clips from 3-week-old pups with primers in exons 21 and 22. (G) Western blot analysis of MEKK4 protein expression in lysates prepared from mouse embryo fibroblasts generated from littermate E14.5 embryos.

caused a perinatal lethality in approximately two-thirds of the pups (Table 1). Of surviving MEKK4^{K1361R} pups, 7% displayed a sacral spina bifida, consisting of a curl proximal to the tail root and an open spinal cord and vertebral canal covered by skin growth shortly after birth (Fig. 4A). Examination of litters immediately after birth revealed dead pups; dead MEKK4^{K1361R} pups frequently exhibited severe open spine defects (Fig. 4B) and occasionally showed rachischisis (Fig. 4C), craniorachischisis (not shown), and omphalocele (open abdominal wall) (Fig. 4D), suggesting that MEKK4^{K1361R} pups were dying from neural tube and body wall closure defects. To further evaluate the cause of mortality in the MEKK4^{K1361R} pups, fetuses were isolated at E18.5 and processed for histology. Compared to littermate controls (Fig. 4E), 20% of MEKK4^{K1361R} fetuses exhibited spina bifida (Fig. 4F). Examination of sections revealed that all organs were grossly normal (not shown). Omphalocele (Fig. 4H) and exencephaly (Fig. 4I) were also observed in E14.5 embryos. Quantitation of NTDs showed that half of the embryos homozygous for the mutation exhibited NTDs (Table 2). Interestingly, 25% of the embryos heterozygous for the mutation had NTDs, suggesting that the mutant MEKK4 interferes with the signaling of the wild-type protein (Table 2). Neural tube closure occurs during embryonic days 8 to 10 (13). TUNEL staining of E9.5 embryos revealed increased apoptosis in the hindbrains of 100% of the exencephalic MEKK4^{K1361R} embryos relative to wild-type littermates (Fig. 4J and K). Apoptosis was not altered in the nonexencephalic MEKK4^{K1361R} embryos (not shown). Enhanced apoptosis in the hindbrain has been previously shown to result in failure of neural

TABLE 1. Genotypes of offspring from heterozygous MEKK4^{wt}/MEKK4^{K1361R} intercrosses

Stage	Total	No. with genotype		
		MEKK4$^{wt/wt}$	MEKK4$^{K1361R/wt}$	MEKK4$^{K1361R/K1361R}$
Postnatal	498	146	306	46
E17.5/E18.5	44	14	18	12
E9.5/E11.5	42	11	17	14

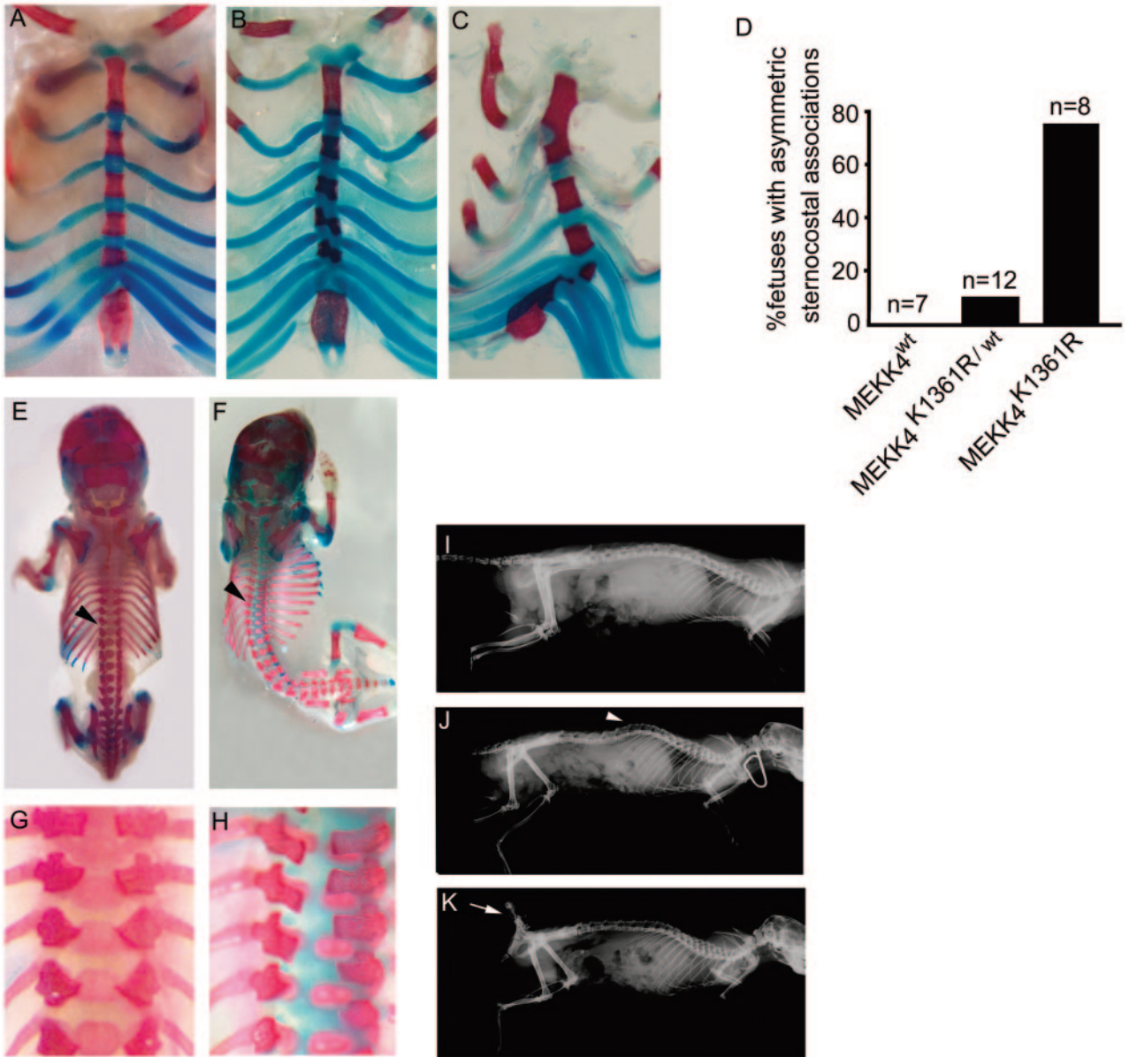

FIG. 3. Skeletal defects in mice expressing kinase-inactive MEKK4^{K1361R}. Bone (Alizarin red) and cartilage (Alcian blue) staining of ribcages from wild-type (A), homozygous knock-in of MEKK4^{K1361R} (B), and heterozygote (C) fetuses isolated at E18.5, showing asymmetric attachment of sternocostal connections. (D) Quantitation of the frequency of rib misalignment in fetuses from heterozygote crosses. Dorsal views of whole animal bone and cartilage staining in wild-type (E and G) and a heterozygous knock-in of MEKK4^{K1361R} (F and H), showing severe curvature of the spine, are shown. Magnification of vertebral columns of wild-type (G) and heterozygous mutant (H) fetuses, showing misalignment of vertebra in the mutant fetus. X-ray films showing scoliosis (J) and an abnormal tail (K) in homozygous knock-in MEKK4^{K1361R} adult mice are compared to the wild type (I). Black arrowheads (E and F) indicate the area of vertebral column seen in the enlarged insets (G and H); the white arrowhead (J) indicates scoliosis; the white arrow (K) indicates bone remodeling in the tail.

tube closure and increased neonatal lethality (16, 29). Our data show a dysregulation of cell death in the hindbrain and suggest that MEKK4 kinase activity plays an antiapoptotic role in embryonic brain development. In summary, these data demonstrate a previously undescribed role for MEKK4 kinase activity in axial skeleton patterning and confirm a previously described role for MEKK4 in neural tube closure (6).

MKK3/6 phosphorylation is decreased in hindbrains of E9.5 MEKK4^{K1361R} embryos. MEKK4 is a MAP3K that activates JNK and p38 MAPKs (11, 31), suggesting that developmental

TABLE 2. Quantitation of NTDs in embryos from heterozygous MEKK4^{wt}/MEKK4^{K1361R} intercrosses

Genotype	Total	No. with phenotype[a]			% of embryos with NTDs
		EX	SB	EX + SB	
MEKK4$^{wt/wt}$	20	0	0	0	0
MEKK4$^{K1361R/wt}$	24	3	1	2	25
MEKK4$^{K1361R/K1361R}$	15	5	2	1	53

[a] EX, exencephaly; SB, spina bifida.

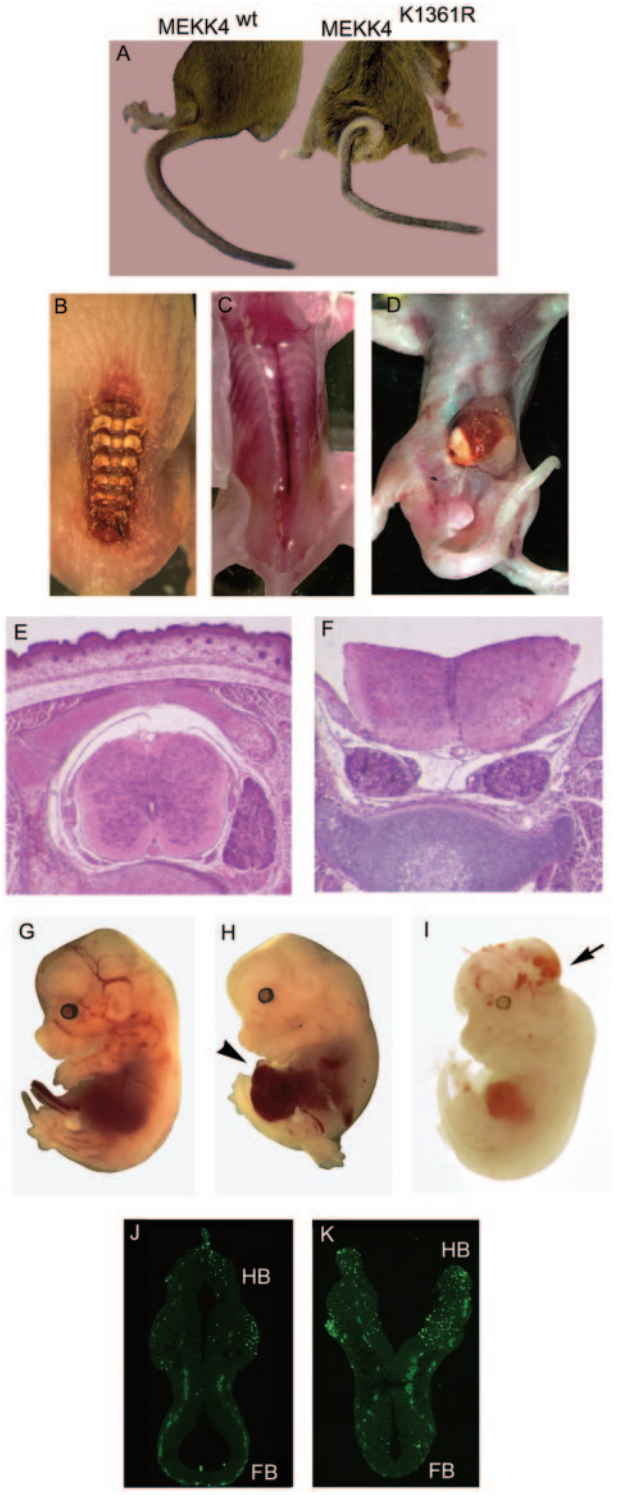

FIG. 4. Neonates homozygous for MEKK4^{K1361R} die at birth due to severe open neural tube and spine defects. (A) Posterior view of a normal adult wild-type mouse and the curly tail-spina bifida phenotype in a mouse homozygous for kinase-inactive MEKK4^{K1361R}. (B) Dorsal view of dead MEKK4^{K1361R} neonate, showing open spine. (C) Dorsal view of dead homozygous MEKK4^{K1361R} neonate, showing rachischisis. (D) Ventral view of dead neonate homozygous for MEKK4^{K1361R}, showing omphalocele. (E and F) Transverse sections taken from paraffin-embedded E18.5 fetuses stained with hematoxylin-eosin. (E) Normal spinal chord in heterozygote littermate control. (F) Open spinal chord in MEKK4^{K1361R} fetus with spina bifida. (G to I) Embryos isolated at E14.5. Normal wild-type embryo (G) and mutant heterozygote embryos with omphalocele (H) or exencephaly (I). The arrowhead (H) indicates omphalocele and the arrow (I) indicates exencephaly. (J and K) TUNEL-labeled 10-μm cryosections from littermate E9.5 embryos. Apoptotic cells are shown in green. (J) The forebrain (FB) and hindbrain (HB) are closed in the wild-type embryo. (K) The hindbrain (HB) remains open and apoptosis is increased in a MEKK4^{K1361R} mutant.

defects in skeletogenesis and neural tube closure in the MEKK4^{K1361R} embryos may be due to disruption of either the JNK or p38 pathways. Although we previously used phospho-specific antibodies for JNK and for p38 to detect phosphorylation in tissue culture cells, the antibodies were not sensitive enough to detect phosphorylation of JNK or p38 in our cryosections from E9.5 embryos. Therefore, we examined phosphorylation of the MAP2Ks that regulate JNK and p38. In sections from wild-type E9.5 embryos, phosphorylation of MKK3/6 was detected in the neuroepithelium of the forebrain and hindbrain and in the mesenchyme (Fig. 5A and AA). Examination of the phosphorylation status of MKK3/6 in hindbrains of exencephalic E9.5 embryos homozygous for MEKK4^{K1361R} revealed a striking loss of phospho-MKK3/6 relative to normal hindbrains from wild-type littermate controls (Fig. 5A, D, AA, and DD). Quantitation of the phosphorylation of MKK3/6 in the neuroepithelium of the hindbrain revealed a 40% decrease in MKK3/6 phosphorylation in mutant hindbrains (Fig. 5G). The loss of MKK3/6 phosphorylation suggests that p38 is chronically inhibited in MEKK4^{K1361R} embryos. A similar loss of phospho-MKK3/6 was also observed in nonexencephalic MEKK4^{K1361R} hindbrains (not shown), indicating that some embryos can escape the loss of MEKK4 kinase activity, consistent with the incomplete penetrance of the mutant phenotype.

TUNEL staining of sections revealed enhanced apoptosis in the hindbrain of exencephalic MEKK4^{K1361R} embryos relative to that in wild-type controls (Fig. 5B and E). Significantly, apoptotic cells were completely excluded from sites with high phospho-MKK3/6 staining (Fig. 5C and F). Phosphorylation of MKK4 was not altered in the mutant hindbrain relative to the wild-type control (Fig. 5H-K). Further, quantitation of phospho-MKK4 fluorescence indicated that phospho-MKK4 levels were not significantly different between wild-type and mutant hindbrains (Fig. 5L). As predicted, phosphorylation of MEK1 and MEK2, MKKs not regulated by MEKK4, was not altered in the mutant hindbrains (Fig. 5M to Q). These data demonstrate that MEKK4^{K1361R} expression selectively disrupted the MKK3/6 and p38 pathway, consistent with MEKK4 regulation of MKK3/6 and p38 being necessary for normal neural tube development.

Upon activation by MKK3/6, p38 translocates to the nucleus where it phosphorylates multiple downstream targets, including the kinase MAPKAPK-2 (28). Perturbation of p38 activation in MEKK4^{K1361R} embryos was further established by examination of phosphorylation by MAPKAPK-2, phosphorylation that occurs directly and exclusively via p38 (28). As shown in Fig. 5R to U, phosphorylation of MAPKAPK-2 was detected in cells lining the ventricles, neuroepithelial cells of the forebrain and hindbrain, and mesenchymal cells of wild-type embryos. Signifi-

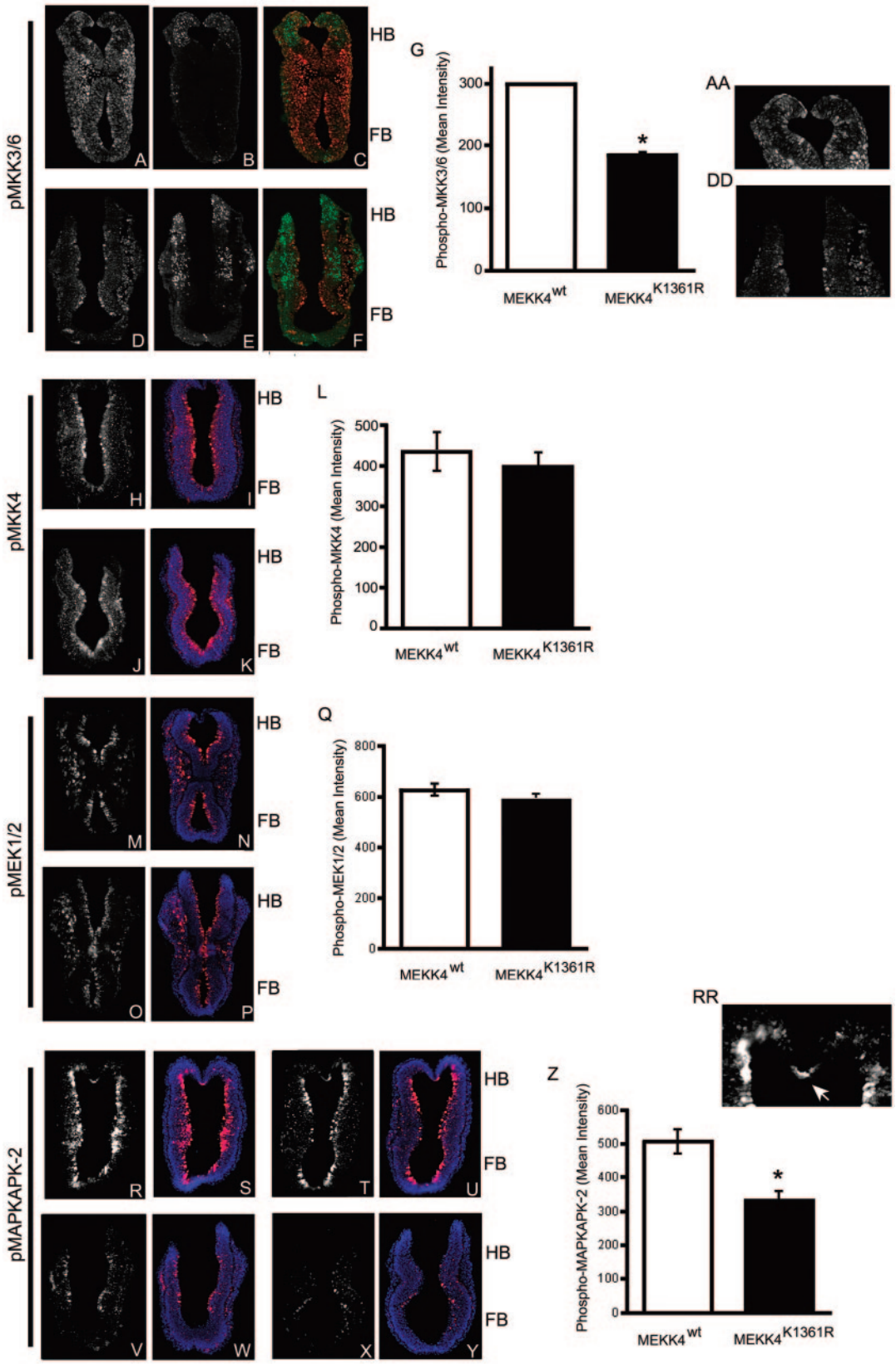

FIG. 5. Inhibition of MKK3/6 and MAPKAPK-2 phosphorylation in MEKK4^{K1361R} hindbrains. Cryosections from wild-type (A to C, H, I, M, N, and R to U) and homozygous MEKK4^{K1361R} (D to F, J, K, O, P, and V to Y) E9.5 embryos isolated from timed heterozygote matings. (A and D) Phosphorylation of MKK3/6 is decreased in the hindbrains of MEKK4^{K1361R} E9.5 embryos relative to wild-type littermates. A phospho-specific antibody for MKK3/6 was used to immunostain sections. (AA and DD) Enlarged insets of panels A and D, showing decreased phospho-MKK3/6

cantly, phosphorylation of MAPKAPK-2 was detected in cells located at the site of neural tube closure in the hindbrain (Fig.5RR). This phosphorylation was significantly decreased in MEKK4^{K1361R} embryos (Fig. 5V and Y). Quantitation of phospho-MAPKAPK-2 fluorescence intensity in the hindbrain revealed a 35% decrease in exencephalic hindbrains (Fig. 5Z), and a 27.5% decrease in phospho-MAPKAPK-2 staining was measured in nonexencephalic MEKK4^{K1361R} hindbrains (not shown). This result is consistent with the diminished MKK3/6 activity in both the exencephalic and nonexencephalic hindbrains; the MEKK4^{K1361R} phenotype is characteristic of many mutations in the developing embryo that demonstrate incomplete penetrance.

Inhibition of the p38 pathway by endogenous MEKK4^{K1361R} expression in mouse embryonic fibroblasts. To confirm the role of MEKK4 in regulating the p38 pathway, we examined primary fibroblasts prepared from MEKK4^{K1361R} and littermate wild-type embryos. A consistent and highly reproducible effect of MEKK4^{K1361R} expression in multiple primary and immortalized MEF preparations was a marked inhibition of p38 activity in cycling cells (Fig. 6A). The inhibition of p38 activity in cycling cells in the presence of 10% serum indicates that p38 is chronically inhibited in nonstressed MEKK4^{K1361R} cells. However, there was no difference in acute p38 stimulation by the inflammatory cytokine TNF-α that does not utilize MEKK4 for p38 activation (Fig. 6B) (38). Phosphorylation of the MAP2Ks MKK3, MKK4, and MKK6 that phosphorylate p38 were also measured. Phosphorylation of MKK4 was not inhibited in MEKK4^{K1361R} cells and P-MKK6 levels were undetectable under these conditions in either wild-type or mutant MEFs (not shown). Similar to our findings with the hindbrains of MEKK4^{K1361R} embryos, phosphorylation of MKK3 was completely inhibited in cycling MEKK4^{K1361R} fibroblasts, whereas TNF-α-stimulated phospho-MKK3 was unaffected (Fig. 6C). These data demonstrate that p38 and MKK3 are chronically repressed in MEKK4^{K1361R} fibroblasts. Reduced phosphorylation of p38 in cycling cells is not due to changes in MKK4 phosphorylation but is attributable to the decreased activation of MKK3 and possibly MKK6. Similar to findings in mutant hindbrains, phosphorylation of MAPKAPK-2 was also inhibited in mutant fibroblasts. There are two isoforms of MAPKAPK-2, a 370-amino-acid form and a larger 400-amino-acid form (28), and phosphorylation of both isoforms was decreased in primary MEKK4^{K1361R} fibroblasts (Fig. 6D). However, phosphorylation of both JNK1/2 and ERK1/2 was similar in wild-type and kinase-inactive MEKK4 cells (Fig. 6D).

As described in Fig. 3 and 5, MEKK4^{K1361R} embryos exhibit increased apoptosis in the hindbrain neuroepithelium. The small heat shock protein HSP27 is phosphorylated by MAPKAPK-2 and promotes stability of the actin cytoskeleton and cell survival (9, 19, 28). Phosphorylation of HSP27 in cycling cells was reduced in MEKK4^{K1361R} fibroblasts relative to wild-type controls, suggesting that MEKK4 regulates steady-state levels of phospho-HSP27 (Fig. 6D). In addition, inhibition of the heat shock response was observed. As shown in Fig. 6E, heat shock-induced activation of p38 is reduced in MEKK4^{K1361R} fibroblasts relative to wild-type controls, whereas JNK activation by heat shock was similar (Fig. 6E). HSP27 phosphorylation in response to heat shock was dramatically reduced in MEKK4^{K1361R} fibroblasts, consistent with the reduction in p38 activity (Fig. 6F). Integrity of the actin microfilaments in MEKK4^{K1361R} fibroblasts was markedly reduced in response to heat shock, resulting in increased cell retraction relative to wild-type MEFs (Fig. 7). Preconditioning of cells at 42°C failed to protect actin filaments in MEKK4^{K1361R} fibroblasts from heat stress at 45°C, consistent with the diminshed phosphorylation of HSP27 at 42C (Fig. 6F and Fig. 7). These data show the functional consequence of the loss of MEKK4 kinase activity in regulation of the actin cytoskeleton controlled by HSP27. The findings demonstrate that MEKK4^{K1361R}-expressing cells are susceptible to specific stresses.

DISCUSSION

Neural tube and skeletal defects are disabling human congenital defects, with neural tube defects being the second most common human birth defect (8, 39). Studies of mouse models that impact neural tube and skeletal development, such as the MEKK4^{K1361R} mouse, provide valuable insight into the mechanisms of these processes. Approximately 75% of embryos homozygous for MEKK4^{K1361R} have skeletal patterning defects, while 50% of the MEKK4 kinase-inactive embryos have neural tube defects including spina bifida and exencephaly. Exencephaly resulted from enhanced apoptosis in the hindbrains of E9.5 mutant embryos, suggesting that MEKK4 plays an antiapoptotic role in the developing hindbrain.

Inhibition of p38 activity in MEKK4^{K1361R} cycling fibro-

in MEKK4^{K1361R} hindbrain. (B and E) TUNEL staining of sections showing enhanced apoptosis in the hindbrain of the MEKK4^{K1361R} embryo. (C and F) Overlay of the phospho-MKK3/6 and TUNEL staining, showing the exclusion of apoptotic cells from areas with high phospho-MKK3/6 immunostaining. Phospho-MKK3/6 staining is in red, and TUNEL staining is in green. (G) Quantitation of mean phospho-MKK3/6 fluorescence intensity in the hindbrain. Data represent the means ± standard error of the mean (SEM) of three samples, each with P values of <0.001, indicating that differences are statistically significant. (H to K) Phosphorylation of MKK4 is similar in wild-type and mutant hindbrains. Phosphorylation of MKK4, shown in red, was detected with a phospho-specific antibody to MKK4; nuclei stained with DAPI are in blue. (L) Quantitation of mean phospho-MKK4 fluorescence intensity in the hindbrain. Data represent the means ± SEM of six samples, each with P values of >0.25, indicating that differences are not statistically significant. (M to P) Phosphorylation of MEK1/2 is similar in wild-type and mutant hindbrains. Phosphorylation of MEK1/2, shown in red, was detected with a phospho-specific antibody to MEK1/2; nuclei are shown in blue. (Q) Quantitation of mean phospho-MEK1/2 fluorescence intensity in the hindbrain. Data represent the means ± SEM of nine wild-type and five mutant samples with P values of >0.15, indicating that differences are not statistically significant. (R to Y) Phosphorylation of MAPKAPK-2 is decreased in the hindbrains of MEKK4^{K1361R} E9.5 embryos relative to that of wild-type littermates. A phospho-specific antibody for MAPKAPK-2, shown in red, was used to immunostain sections; nuclei are shown in blue. (Z) Quantitation of mean phospho-MAPKAPK-2 fluorescence intensity in hindbrain. Data represent the means ± SEM of nine wild-type and eight mutant samples with P values of <0.001, indicating that differences are statistically significant. (RR) Enlarged inset of R, showing localization of phospho-MAPKAPK-2 at the site of neural tube closure in the wild-type hindbrain. Forebrain (FB) and hindbrain (HB) are closed in the wild-type embryo. The hindbrain remains open in the MEKK4^{K1361R} mutants. *, $P < 0.001$. The white arrow indicates the site of hindbrain closure.

blasts corroborates the studies in embryos that MEKK4 is a primary MAP3K for controlling endogenous p38 activity. MEKK4 is important for control of p38 by serum growth factors, independent of p38 stimulation by the inflammatory cytokine TNF-α. The mechanism for p38 inhibition in cycling cells is inhibition of the activation of MKK3/6, which are direct substrates for MEKK4.

HSP27, which is downstream of p38, is known to protect cells from apoptosis. HSP27 phosphorylation in cycling MEKK4^{K1361R} cells is markedly inhibited, consistent with the reduced activation of p38 and MAPKAPK-2. Further, heat shock-induced phosphorylation of both p38 and HSP27 was reduced in MEKK4^{K1361R} cells, suggesting an important role for MEKK4 in the heat shock-induced stress response. We could not detect phospho-HSP27 in embryo cryosections, due to the insensitivity of the available antibodies but not due to lack of expression, as HSP27 message is constitutively expressed in the developing central nervous system (21, 35). As an in vitro validation of MEKK4 regulation of HSP27, MEKK4^{K1361R} MEFs exposed to heat shock demonstrated a reduction in the stability of actin microfilaments.

p38 knockout mice with distinctly different phenotypes have been created by multiple laboratories, but there have been no reports in these studies of neural tube closure defects (1, 2, 14, 23, 32). However, the existence of four p38 family members may allow redundant signaling pathways to compensate for the loss of a single p38 isoform. An antiapoptotic function for p38 has been shown in vitro for macrophages and differentiating neurons (20, 26). Cleavage of MKK3 by lethal factor induces macrophage apoptosis by inhibiting p38-dependent expression of selective NF-κB target genes that protect activated macrophages from apoptosis (26). During development of cerebellar granule neurons, calcium influx activates p38, leading to the activation of MEF2, MEF2-dependent gene transcription, and cell survival (20). Expression of a dominant negative p38 promoted apoptosis of differentiating neurons that was rescued by a constitutively activated form of MEF2C, consistent with a role for p38 in transcriptional control of antiapoptotic proteins (25). These studies are consistent with our findings that MEKK4 regulates MKK3/p38/MAPKAPK-2 during development, serving a protective, antiapoptotic role.

Concurrent loss of JNK1 and JNK2 protein expression has been shown to result in defective neural tube development manifested primarily as exencephaly (30). Significantly, this phenotype was not observed in single JNK knockout animals but required the deletion of isoforms 1 and 2 (18, 30). Exencephaly in the JNK1/2 dual-knockout embryos was due to enhanced apoptosis in the forebrain and decreased apoptosis in the hindbrain (18). In comparison, we observed increased apoptosis in the hindbrains of MEKK4^{K1361R} mice, while MKK4 signaling was not inhibited in MEKK4^{K1361R} fibroblasts or hindbrains. These differences clearly indicate that loss of MEKK4 kinase activity does not mimic the JNK knockout. The developmental defects observed with MEKK4^{K1361R} mice are due to mechanisms, in part involving inhibited p38 activity. We cannot rule out a contribution of JNK dysregulation in the MEKK4^{K1361R} phenotype, but there is no measurable loss of phospho-MKK4 in the developing neuroepithelium of MEKK4^{K1361R}-expressing mice.

MEKK4 is a large 180-kDa protein with a single catalytic domain but with multiple interaction domains that have been shown to bind Rac, Cdc42, Ccd1, Axin, and GADD45α, -β, and -γ (11, 22, 37). To preserve protein interactions and preclude compensation by other proteins, we used a knock-in strategy to create a point mutation in MEKK4, substituting the active site lysine and selectively inhibiting kinase activity. This mutant mouse enables us to ascertain effects that are solely attributable to a loss of kinase activity, as opposed to deletion of the MEKK4 gene. As predicted, overlapping phenotypes were observed for the MEKK4 knockout and the MEKK4 kinase-inactive mouse. Common features are reduced phosphorylation of p38 in cycling fibroblasts and increased embryonic lethality with neural tube closure defects. Chi et al. attributed the neural tube defects to a very modest decrease in MKK4 phosphorylation without a change in JNK phosphorylation (5, 6). We observed a significantly stronger phenotype with additional defects in the MEKK4^{K1361R} mouse. The dominant phenotype of MEKK4^{K1361R} mice with severe skeletal patterning defects including rib malformations and scoliosis was not described for MEKK4 knockout mice. Also, MEKK4^{K1361R} mice are infertile, unlike MEKK4 knockout mice, which have normal reproductive capacity (5). Some of the differences in the phenotypes of MEKK4^{K1361R} knock-in and MEKK4 knockout mice may be due to differences in genetic backgrounds. Studies of MEKK4^{K1361R} knock-in mice were performed with a mixed 129–C57BL/6 background; the studies of the MEKK4 knockout were performed on both a mixed 129–C57BL/6 background and a C57BL/6 background (5, 6). It is our belief that a kinase-inactive MEKK4 protein, expressed at levels similar to that of the wild-type kinase, is a better indicator of the function of MEKK4 kinase signaling than a null mutant. The behavior of the MEKK4^{K1361R} mutant is much like that predicted for a high-affinity, selective inhibitor of MEKK4. The mutant MEKK4 protein occupies its space in the cell, and expression is from the endogenous gene by the MEKK4 promoter.

It is important to contrast the MEKK4 kinase-inactive phenotype to that of knockouts for downstream kinases controlled by MEKK4. MAP3Ks provide selectivity for activation of MAPKs by upstream stimuli, and there are multiple MAP3Ks that regulate the MKK3/MKK6/p38 pathway (15). The inhibition of serum, but not TNF-α activation of p38 in MEKK4^{K1361R} fibroblasts, demonstrates the selective role of MEKK4 in regulating the p38 pathway. For this reason, the MEKK4^{K1361R} phenotype will not be strictly mimicked by the MKK3/MKK6, p38, or MAPKAPK-2 knockouts. Similarly, MAPKAPK-2 is only one of many p38 substrates; therefore, the MAPKAPK-2 knockout is phenotypically different from the p38 knockout or MEKK4^{K1361R} knock-in. For example, the MAPKAPK-2 knockout mouse shows protection from many pathophysiological stress stimuli that induce expression of TNF-α or interleukin-1 (17), but it is otherwise overtly normal and fertile. This contrasts with p38α knockouts that have vascular, hematopoietic, and placental defects (14), even though MAPKAPK-2 is clearly a p38 substrate. Similarly, kinase-inactive MEKK4 mice have both skeletal patterning and neurulation dysregulation, a phenotype not observed with any MAPK knockout but observed with the ablation of the scaffolding proteins TRAF4 and disheveled-2 (12, 27). Our results suggest that MAP3K kinase-inactive knock-ins will aid in defining the

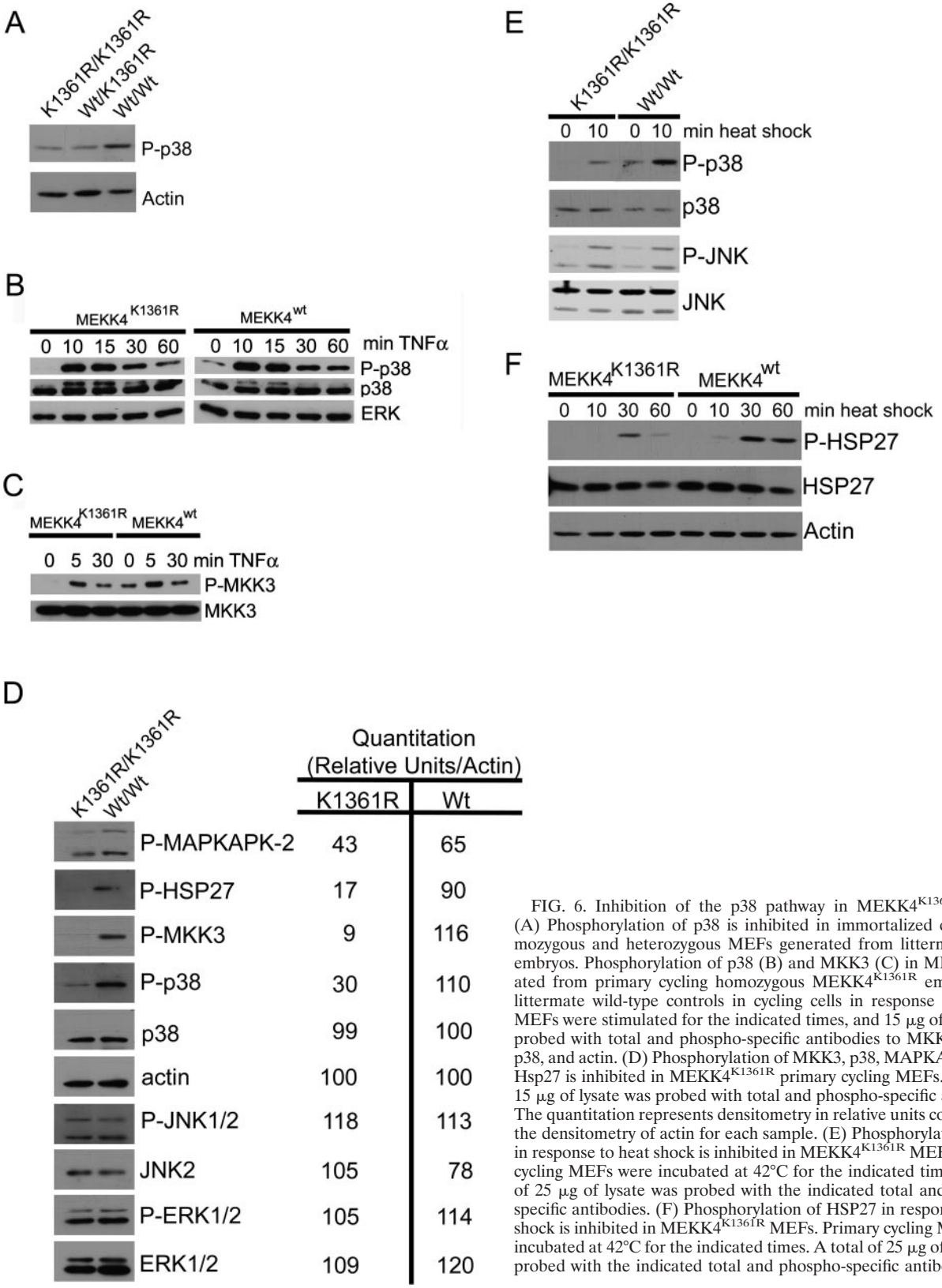

FIG. 6. Inhibition of the p38 pathway in MEKK4^{K1361R} MEFs. (A) Phosphorylation of p38 is inhibited in immortalized cycling homozygous and heterozygous MEFs generated from littermate E14.5 embryos. Phosphorylation of p38 (B) and MKK3 (C) in MEFs generated from primary cycling homozygous MEKK4^{K1361R} embryos and littermate wild-type controls in cycling cells in response to TNF-α. MEFs were stimulated for the indicated times, and 15 μg of lysate was probed with total and phospho-specific antibodies to MKK3, MKK4, p38, and actin. (D) Phosphorylation of MKK3, p38, MAPKAPK-2, and Hsp27 is inhibited in MEKK4^{K1361R} primary cycling MEFs. A total of 15 μg of lysate was probed with total and phospho-specific antibodies. The quantitation represents densitometry in relative units compared to the densitometry of actin for each sample. (E) Phosphorylation of p38 in response to heat shock is inhibited in MEKK4^{K1361R} MEFs. Primary cycling MEFs were incubated at 42°C for the indicated times. A total of 25 μg of lysate was probed with the indicated total and phospho-specific antibodies. (F) Phosphorylation of HSP27 in response to heat shock is inhibited in MEKK4^{K1361R} MEFs. Primary cycling MEFs were incubated at 42°C for the indicated times. A total of 25 μg of lysate was probed with the indicated total and phospho-specific antibodies.

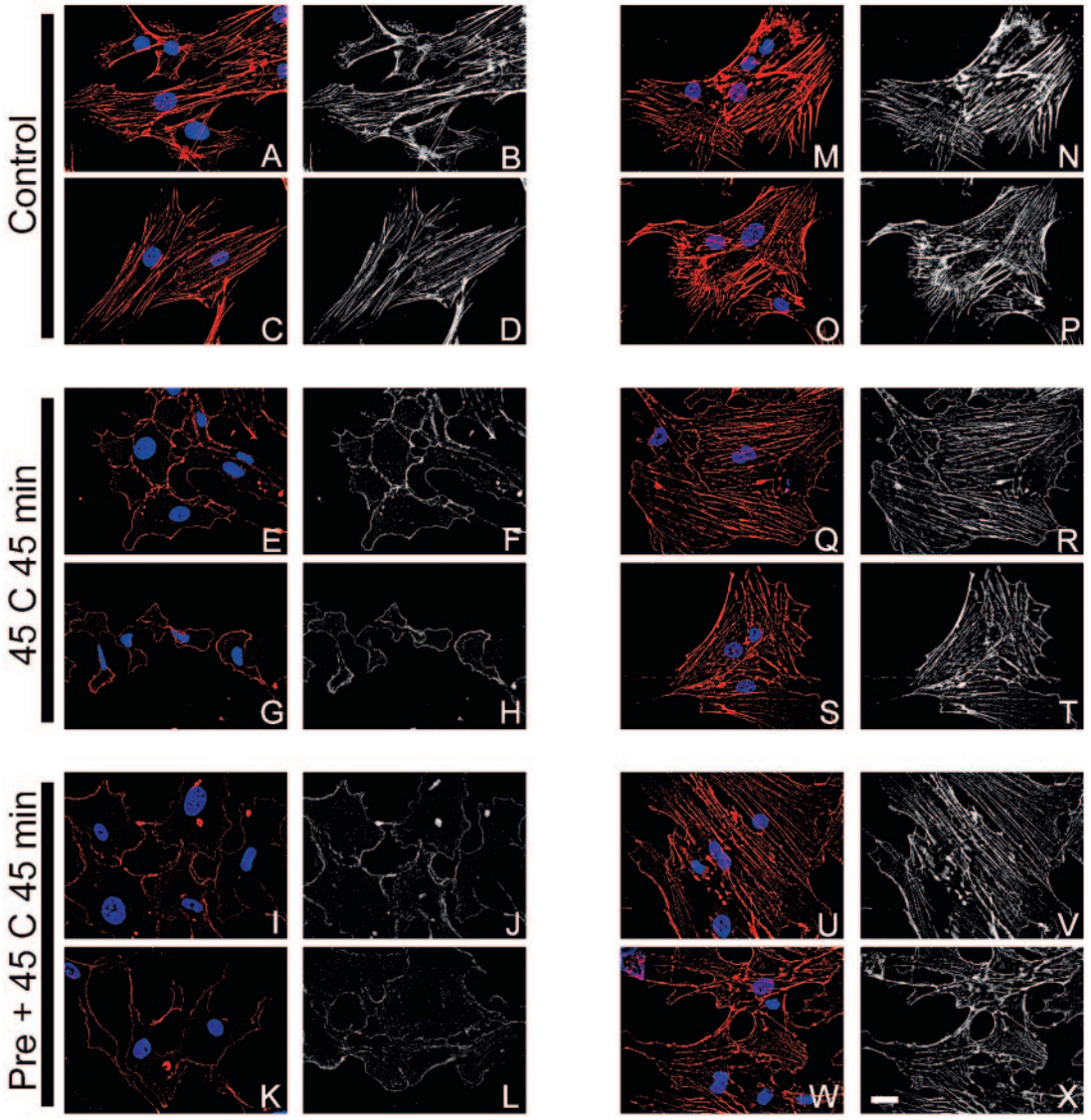

FIG. 7. Increased thermosensitivity of actin microfilaments in primary MEKK4^{K1361R} fibroblasts. Primary fibroblasts from littermate MEKK4^{K1361R} (A to L) or wild-type (M to X) embryos were plated on coverslips. Cells were maintained at 37°C (A to D and M to P), incubated at 45°C for 45 min (E to H and Q to T), or heated at 42°C for 30 min (preconditioning), followed by recovery for 24 h at 37°C and heat shock at 45°C for 45 min (I to L and U to X). Cells were fixed and stained with rhodamine phalloidin to detect polymerized actin (red) and DAPI to stain nuclei (blue). Two sample fields of deconvolved 0.1-μm sections are shown. Black-and-white images show polymerized actin alone. Bar, 25 μM.

complexity of MAPK integration with developmental and physiological responses that are not readily apparent with ablation of MAPK expression (15).

ACKNOWLEDGMENTS

These studies were supported by NIH grants GM30324 and DK37871.

We have no financial conflicts of interest related to these studies.

We thank Pamela J. Cuevas for her expertise in evaluation of the X-ray images. We also acknowledge the technical assistance of Virginia Godfrey and the Lineberger Cancer Center Histopathology Core. We also thank Yongqin Wu for her work on E10.5 in situ hybridizations. We thank G. T. Rosenthal of the UCHSC for technical assistance with the mouse colony.

REFERENCES

1. **Adams, R. H., A. Porras, G. Alonso, M. Jones, K. Vintersten, S. Panelli, A. Valladares, L. Perez, R. Klein, and A. R. Nebreda.** 2000. Essential role of p38α MAP kinase in placental but not embryonic cardiovascular development. Mol. Cell **6:**109–116.
2. **Allen, M., L. Svensson, M. Roach, J. Hambor, J. McNeish, and C. A. Gabel.** 2000. Deficiency of the stress kinase p38α results in embryonic lethality: characterization of the kinase dependence of stress responses of enzyme-deficient embryonic stem cells. J. Exp. Med. **191:**859–870.
3. **Bhasin, N., E. Kernick, X. Luo, H. E. Seidel, E. R. Weiss, and J. M. Lauder.** 2004. Differential regulation of chondrogenic differentiation by the serotonin 2B receptor and retinoic acid in the embryonic mouse hindlimb. Dev. Dyn. **230:**201–209.
4. **Brancho, D., N. Tanaka, A. Jaeschke, J. J. Ventura, N. Kelkar, Y. Tanaka, M. Kyuuma, T. Takeshita, R. A. Flavell, and R. J. Davis.** 2003. Mechanism of p38 MAP kinase activation in vivo. Genes Dev. **17:**1969–1978.
5. **Chi, H., B. Lu, M. Takekawa, R. J. Davis, and R. A. Flavell.** 2004.

GADD45β/GADD45γ and MEKK4 comprise a genetic pathway mediating STAT4-independent IFNγ production in T cells. EMBO J. **23:**1576–1586.
6. **Chi, H., M. R. Sarkisian, P. Rakic, and R. A. Flavell.** 2005. Loss of mitogen-activated protein kinase kinase kinase 4 (MEKK4) results in enhanced apoptosis and defective neural tube development. Proc. Natl. Acad. Sci. USA **102:**3846–3851.
7. **Compagni, A., M. Logan, R. Klein, and R. H. Adams.** 2003. Control of skeletal patterning by ephrin B1-EphB interactions. Dev. Cell **5:**217–230.
8. **Copp, A. J., N. D. Greene, and J. N. Murdoch.** 2003. The genetic basis of mammalian neurulation. Nat. Rev. Genet. **4:**784–793.
9. **Garrido, C., S. Gurbuxani, L. Ravagnan, and G. Kroemer.** 2001. Heat shock proteins: endogenous modulators of apoptotic cell death. Biochem. Biophys. Res. Commun. **286:**433–442.
10. **Garrington, T. P., and G. L. Johnson.** 1999. Organization and regulation of mitogen-activated protein kinase signaling pathways. Curr. Opin. Cell Biol. **11:**211–218.
11. **Gerwins, P., J. L. Blank, and G. L. Johnson.** 1997. Cloning of a novel mitogen-activated protein kinase kinase kinase, MEKK4, that selectively regulates the c-Jun amino terminal kinase pathway. J. Biol. Chem. **272:**8288–8295.
12. **Hamblet, N. S., N. Lijam, P. Ruiz-Lozano, J. Wang, Y. Yang, Z. Luo, L. Mei, K. R. Chien, D. J. Sussman, and A. Wynshaw-Boris.** 2002. Dishevelled 2 is essential for cardiac outflow tract development, somite segmentation and neural tube closure. Development **129:**5827–5838.
13. **Harris, M. J., and D. M. Juriloff.** 1999. Mini-review: toward understanding mechanisms of genetic neural tube defects in mice. Teratology **60:**292–305.
14. **Ihle, J. N.** 2000. The challenges of translating knockout phenotypes into gene function. Cell **102:**131–134.
15. **Johnson, G. L., H. G. Dohlman, and L. M. Graves.** 2005. MAPK kinase kinases (MKKKs) as a target class for small-molecule inhibition to modulate signaling networks and gene expression. Curr. Opin. Chem. Biol. **9:**325–331.
16. **Juriloff, D. M., and M. J. Harris.** 2000. Mouse models for neural tube closure defects. Hum. Mol. Genet. **9:**993–1000.
17. **Kotlyarov, A., A. Neininger, C. Schubert, R. Eckert, C. Birchmeier, H. D. Volk, and M. Gaestel.** 1999. MAPKAP kinase 2 is essential for LPS-induced TNF-alpha biosynthesis. Nat. Cell Biol. **1:**94–97.
18. **Kuan, C. Y., D. D. Yang, D. R. Samanta Roy, R. J. Davis, P. Rakic, and R. A. Flavell.** 1999. The Jnk1 and Jnk2 protein kinases are required for regional specific apoptosis during early brain development. Neuron **22:**667–676.
19. **Lavoie, J. N., H. Lambert, E. Hickey, L. A. Weber, and J. Landry.** 1995. Modulation of cellular thermoresistance and actin filament stability accompanies phosphorylation-induced changes in the oligomeric structure of heat shock protein 27. Mol. Cell. Biol. **15:**505–516.
20. **Mao, Z., A. Bonni, F. Xia, M. Nadal-Vicens, and M. E. Greenberg.** 1999. Neuronal activity-dependent cell survival mediated by transcription factor MEF2. Science **286:**785–790.
21. **Michaud, S., R. Marin, and R. M. Tanguay.** 1997. Regulation of heat shock gene induction and expression during Drosophila development. Cell. Mol. Life Sci. **53:**104–113.
22. **Mita, H., J. Tsutsui, M. Takekawa, E. A. Witten, and H. Saito.** 2002. Regulation of MTK1/MEKK4 kinase activity by its N-terminal autoinhibitory domain and GADD45 binding. Mol. Cell. Biol. **22:**4544–4555.
23. **Mudgett, J. S., J. Ding, L. Guh-Siesel, N. A. Chartrain, L. Yang, S. Gopal, and M. M. Shen.** 2000. Essential role for p38α mitogen-activated protein kinase in placental angiogenesis. Proc. Natl. Acad. Sci. USA **97:**10454–10459.
24. **Neubuser, A., H. Koseki, and R. Balling.** 1995. Characterization and developmental expression of Pax9, a paired-box-containing gene related to Pax1. Dev. Biol. **170:**701–716.
25. **Okamoto, S., D. Krainc, K. Sherman, and S. A. Lipton.** 2000. Antiapoptotic role of the p38 mitogen-activated protein kinase-myocyte enhancer factor 2 transcription factor pathway during neuronal differentiation. Proc. Natl. Acad. Sci. USA **97:**7561–7566.
26. **Park, J. M., F. R. Greten, Z. W. Li, and M. Karin.** 2002. Macrophage apoptosis by anthrax lethal factor through p38 MAP kinase inhibition. Science **297:**2048–2051.
27. **Regnier, C. H., R. Masson, V. Kedinger, J. Textoris, I. Stoll, M. P. Chenard, A. Dierich, C. Tomasetto, and M. C. Rio.** 2002. Impaired neural tube closure, axial skeleton malformations, and tracheal ring disruption in TRAF4-deficient mice. Proc. Natl. Acad. Sci. USA **99:**5585–5590.
28. **Roux, P. P., and J. Blenis.** 2004. ERK and p38 MAPK-activated protein kinases: a family of protein kinases with diverse biological functions. Microbiol. Mol. Biol. Rev. **68:**320–344.
29. **Ruland, J., G. S. Duncan, A. Elia, I. del Barco Barrantes, L. Nguyen, S. Plyte, D. G. Millar, D. Bouchard, A. Wakeham, P. S. Ohashi, and T. W. Mak.** 2001. Bcl10 is a positive regulator of antigen receptor-induced activation of NF-κB and neural tube closure. Cell **104:**33–42.
30. **Sabapathy, K., W. Jochum, K. Hochedlinger, L. Chang, M. Karin, and E. F. Wagner.** 1999. Defective neural tube morphogenesis and altered apoptosis in the absence of both JNK1 and JNK2. Mech. Dev. **89:**115–124.
31. **Takekawa, M., F. Posas, and H. Saito.** 1997. A human homolog of the yeast Ssk2/Ssk22 MAP kinase kinase kinases, MTK1, mediates stress-induced activation of the p38 and JNK pathways. EMBO J. **16:**4973–4982.
32. **Tamura, K., T. Sudo, U. Senftleben, A. M. Dadak, R. Johnson, and M. Karin.** 2000. Requirement for p38α in erythropoietin expression: a role for stress kinases in erythropoiesis. Cell **102:**221–231.
33. **Uhlik, M. T., A. N. Abell, N. L. Johnson, W. Sun, B. D. Cuevas, K. E. Lobel-Rice, E. A. Horne, M. L. Dell'Acqua, and G. L. Johnson.** 2003. Rac-MEKK3-MKK3 scaffolding for p38 MAPK activation during hyperosmotic shock. Nat. Cell Biol **5:**1104–1110.
34. **Wada, T., and J. M. Penninger.** 2004. Mitogen-activated protein kinases in apoptosis regulation. Oncogene **23:**2838–2849.
35. **Walsh, D., Z. Li, Y. Wu, and K. Nagata.** 1997. Heat shock and the role of the HSPs during neural plate induction in early mammalian CNS and brain development. Cell. Mol. Life Sci. **53:**198–211.
36. **Wilkinson, D. G., S. Bhatt, and B. G. Herrmann.** 1990. Expression pattern of the mouse T gene and its role in mesoderm formation. Nature **343:**657–659.
37. **Wong, C. K., W. Luo, Y. Deng, H. Zou, Z. Ye, and S. C. Lin.** 2004. The DIX domain protein coiled-coil-DIX1 inhibits c-Jun N-terminal kinase activation by Axin and dishevelled through distinct mechanisms. J. Biol. Chem. **279:**39366–39373.
38. **Yang, J., Y. Lin, Z. Guo, J. Cheng, J. Huang, L. Deng, W. Liao, Z. Chen, Z. Liu, and B. Su.** 2001. The essential role of MEKK3 in TNF-induced NF-κB activation. Nat. Immunol. **2:**620–624.
39. **Zelzer, E., and B. R. Olsen.** 2003. The genetic basis for skeletal diseases. Nature **423:**343–348.